Available online at www.sciencedirect.com

ScienceDirect

Advances in Space Research xxx (xxxx) xxx

ADVANCES IN SPACE RESEARCH (a COSPAR publication)

www.elsevier.com/locate/asr

A high energy cosmic-ray and gamma-ray observatory at the Moon South Pole: the MoonRay concept ☆

P.S. Marrocchesi *

Dept. of Physical Sciences, Earth and Environment, University of Siena, V. Roma 56, 53100, Siena, Italy
INFN sez. di Pisa, Largo B.Pontecorvo 3, 56127, Pisa, Italy

Received 9 April 2025; received in revised form 19 September 2025; accepted 17 October 2025

Abstract

The MoonRay project is pursuing a concept study of a permanent cosmic-ray and gamma-ray observatory on the Moon, in view of the current plans for the implementation of habitats on our satellite. The idea is to build a modular telescope that will be able not only to overcome the limitations, in available power and weight, of the present generation of cosmic-ray instruments in Low Earth Orbit, but also to operate as a powerful high energy gamma-ray observatory from a vantage point at the South Pole of the Moon. An array of fully independent modules (towers), with limited individual size and mass, can provide a geometric factor more than one order of magnitude larger than instruments in flight, or planned to be operational within the decade. The modular telescope is designed to be deployed progressively, along a series of lunar missions, while collecting meaningful scientific data during the intermediate stages of its implementation. Power will be made available by the facilities that will maintain the lunar habitats. With a geometric factor close to 15 m^2 sr and about 8 times larger sensitive area than FERMI-LAT Atwood et al. (2009), MoonRay will be able to carry out a very rich observational program over a time span of a few decades with the exploration of the CR "knee" to about 10 PeV and the observation of the Southern Sky with gamma rays, from GeV to multi-TeV.

Each tower is equipped with three main instruments. Leveraging on an innovative two-layered array of pixelated Low Gain Avalanche Diode (LGAD) sensors, with sub-ns time resolution, a combined Charge and Time-of-Flight detector (CD-ToF) identifies individual cosmic elements, while providing an unprecedented rejection power against back-scattered radiation from the calorimeter. It is followed by a tracker (equipped with absorbers to provide photon conversion), and by a thick calorimeter of 3 cm side cubic crystals (55 radiation lengths, 3 proton interaction lengths at normal incidence) with an energy resolution of 30–40% (2%) for protons (electrons) and a proton/electron rejection in excess of 10^5. The design of each instrument contains innovative solutions that are well within the reach of the present technology.

A test campaign of prototype arrays with 3 mm × 3 mm LGAD pixels was recently carried out at CERN with a fragmented Pb beam. Results will be reported showing a preliminary time resolution close to 100 ps.

Keywords: Lunar telescope; Cosmic rays; Gamma rays

1. Introduction

During the last decade, a new generation of space instruments have carried out direct measurements of cosmic-ray phenomena with unprecedented precision, significantly expanding the reach of direct observations above the

☆ This article is part of a special issue entitled: 'SI: Astrophysics of cosmic rays' published in Advances in Space Research.

* Address: Dept. of Physical Sciences, Earth and Environment, University of Siena, V. Roma 56, 53100, Siena, Italy.
E-mail address: marrocchesi@unisi.it.

https://doi.org/10.1016/j.asr.2025.10.076
0273-1177/

atmosphere and discovering unexpected features in the energy spectra of charged cosmic rays.

Deviations of the fluxes from a pure power-law spectrum above a few hundred GeV/n have been observed recently by balloon and space-borne experiments including ATIC (Panov et al., 2007), CREAM (Ahn et al., 2010), PAMELA (Adriani et al., 2011), AMS-02 (Aguilar et al., 2015), CALET (Adriani et al., 2019), DAMPE (An et al., 2019), and NUCLEON (Atkin et al., 2018) (more contributions can be found in the reference listing).

The observation of a "spectral hardening" in the proton and helium rigidity spectra was unexpected. The proton flux has been found to exhibit a smooth and progressive increase of the spectral index starting above a few hundred GV and continuing up to ~10 TV. At even higher energies this trend changes and – again in an unexpected way – both spectra undergo a "softening", as shown by the subsequent observations of proton and helium fluxes at the multi-TeV scale carried out by DAMPE (An et al., 2019) and CALET (Adriani et al., 2022).

The presence of a "proton bump" came as a surprise and triggered a number of theoretical speculations invoking different scenarios as the dominance of one (or more) nearby supernova remnant(s) (SNR), the confinement and gradual release of CRs from the source, and the possibility of an anomalous diffusive regime near the acceleration sites. We cite here only a small subset of the wide spectrum of recent model of CR acceleration and propagation, including: (Zatsepin and Sokolskaya, 2006; Blasi et al., 2012; Vladimirov et al., 2012; Aloisio and Blasi, 2013; Bernard et al., 2013; Thoudam and Hörandel, 2014; Kawanaka and Yanagita, 2018; Tomassetti, 2015; Caprioli et al., 2021; Cristofari et al., 2022; Evoli et al., 2021; Malkov et al., 2024; Lipari and Vernetto, 2025).

A systematic campaign of direct measurements of secondary-to-primary and primary-to-primary ratios provided important input to the study of CR propagation in the Galaxy. Furthermore, precision measurements of the fluxes of cosmic elements heavier than He clearly indicated that primary and secondary cosmic elements exhibit different rigidity dependencies Aguilar et al. (2020). The emergence of this new rich phenomenology, together with the discovery of breaks in the spectra, challenge the conventional interpretation of CR spectra in terms of simple power-laws and calls for an extension of the observations to PeV energies. This is a region where the "knee", a spectral anomaly discovered more than half a century ago in the all-particle cosmic-ray flux, is located, approximately one decade around 3–4 PeV, with a spectral index break from ~2.7 (below 10^{14}eV) to ~3.1.

2. The experimental challenge

As it is well known, the maximum weight and power available on a payload represent the two main limitations to the possibility of deploying a large area instrument with a sufficient collecting power to accumulate, in a reasonable mission timescale (10–15 years), the statistics needed to study the "knee".

At present, magnetic spectrometers in space are limited to a Maximum Detectable Rigidity (MDR) of a few TV, as it is the case of AMS-02, in operation on the ISS since 2011. After the conclusion of PAMELA operations, AMS-02 is the only instrument in orbit with the ability to separate electrons from positrons by measuring the sign of their charge. This allows AMS-02 to carry out separate measurements of the high-energy spectra of positrons and anti-protons, providing important input to the search of Dark Matter via the observation of final states containing anti-particles.

On the other hand, experiments that measure the energy of the incident CR with a calorimeter can reach higher energies. This is the case of two experiments in Low Earth Orbit (LEO): CALET (on the ISS) and DAMPE (on a satellite), both launched in 2015, that have provided precision measurements of CR spectra and extended the range of direct measurements above 100 TeV. However, the calorimetric instruments in operation at this time, though capable of measuring single-particle energies up to the PeV scale and currently exploring the region from 100 TeV to 1 PeV, are unable to provide statistically relevant information on the region around the "knee" (approximately from 10^{16}eV to 10^{17}eV) due to their limited collection power caused by the dramatic reduction of the fluxes (by about a factor of 50 per decade) with increasing energy. Charting this energy region with direct measurements would allow to study the elemental composition of cosmic rays at the "knee", closing the gap with the indirect observations provided by ground experiments.

This challenging goal calls for an experimental apparatus with a geometric acceptance of at least 3 m^2sr, i.e., more than one order of magnitude larger than the space instruments in flight at present. This objective is being pursued by a large-acceptance payload HERD (Dong et al., 2018), designed to be installed aboard the Chinese Space Station. According to the present expectations, the mission would become operational before the end of the decade. On a longer time scale, a next generation of large missions, is under study for a possible launch around the mid of the century. They include AMS100 (Schael et al., 2019) and ALADinO (Adriani et al., 2022), two large instruments that have been proposed for long-term observations at the Lagrangian point L2.

As an alternative to a single payload carrying a heavy large area instrument, one could consider a constellation of many satellites in LEO. While this approach might look appealing for the study of high energy gamma-rays with an instrument equipped with a thin calorimeter (as is is the case of FERMI-LAT with only 8 radiation lengths at normal incidence) this approach would be completely inadequate for VHE cosmic rays. This is due to the fact that high energy measurements require a much larger (5–6 times) calorimetric depth and a large active volume (to minimize hadronic shower leaks) wherein precise calibra-

tions would be carried out, allowing a good control of the systematic errors. Instead, keeping the systematics of a cluster of independent CR instruments under control may not be so straitforward, as it can be seen by comparing the CR flux data measured by the latest generation of instruments in orbit, which show significant differences most likely due to different sources of systematics.

Another possibility is to build a large "ground telescope" on the Moon. *Modularity* is the key idea of MoonRay (Marrocchesi, 2023) with the design of a telescope, segmented into relatively lightweight modules, that could be installed progressively, over a long-term program of lunar missions, until the required geometric acceptance is achieved. This approach is radically different from current orbital missions, whereby the experimental apparatus is assembled on the ground before launch and its maximum geometric acceptance is fixed and heavily penalized by weight and power limitations. The MoonRay instrument is segmented into units called "towers" (Fig. 2). Each tower is a completely independent functional unit. The sensitive area of the telescope is extended during consecutive missions with the deployment of extra towers, while keeping the instrument operational in between two subsequent phases of its upgrade.

The MoonRay concept has been formulated *assuming* an hypothetical scenario where lunar habitats would be in operation. This implies that the lunar power infrastructures, in charge of life support for the astronauts and their activities, would be able to sustain a power budget by far much larger than the amount required for the telescope, which is typically limited to a few kW. We will come back to this point in a later section.

A second advantage is the low lunar gravity (about 1/6 than on Earth), which facilitates the installation of modules of reasonable size and weight. The study of a modular apparatus (Fig. 1) operating on the Moon and designed to carry out direct observations of charged cosmic radiation and high-energy gamma rays is briefly described in the following. Its development requires the implementation of some innovative ideas, yet remaining within the framework of technologies that are already available.

3. Outline of the MoonRay cosmic radiation telescope

The design of the MoonRay telescope relies on recent advances in high-energy particle instrumentation. Each tower includes three main instruments:

- a **particle identifier (CD-ToF)**, integrating high resolution Time-of-Flight (ToF) capabilities into a charge detector (CD), for the simultaneous measurement of the electric charge and of the time of arrival of the incident particle. This is a newly developed instrument based on Low Gain Avalanche Diodes (LGAD) sensors with sub-ns time resolution. It allows a clean charge identification of the CR incident particle thanks to an efficient rejection of the copious back-scattering background generated by its interaction with the calorimeter;
- a **modular tracking system (MT)** based on semiconductor position detectors (interspaced with thin photon absorbers) or, alternatively, on a scintillating fiber tracker with silicon photodetectors (SiPM) readout;
- a **homogeneous calorimeter (MCAL)** segmented in layers of reasonable size and weight, each consisting of a 3D array of scintillating crystals readout by photodiodes.

The "core" of the telescope consists of a bidimensional array of towers (10×10 as baseline configuration, or up to 16×16, as shown in Fig. 3. "Lateral walls" extend the coverage to the four lateral sides. As shown in Fig. 2, this is

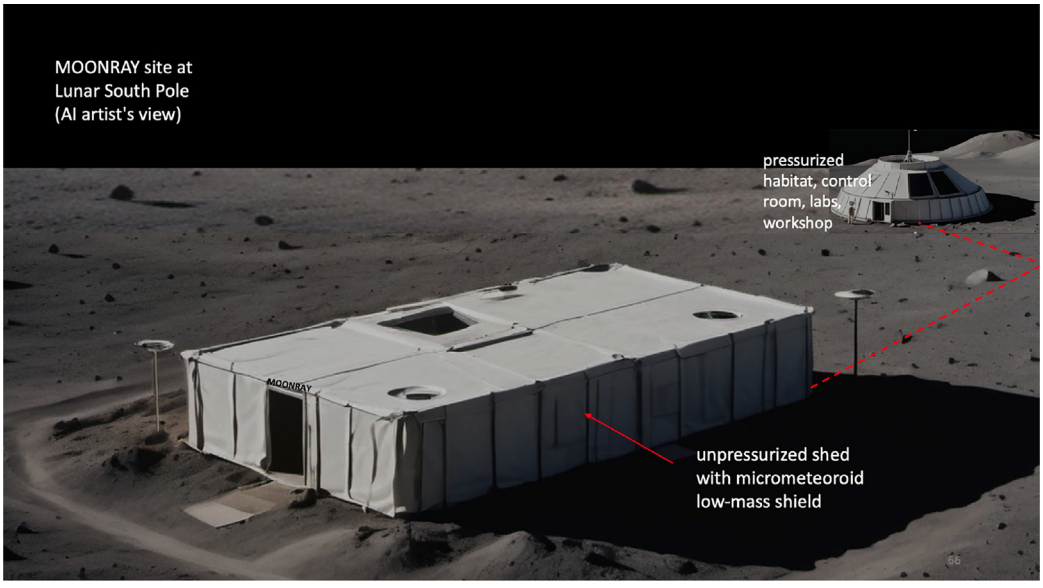

Fig. 1. Artist's view of an unpressurized shed hosting the proposed MoonRay telescope and of a nearby pressurized habitat with the control room and laboratories (top right).

Please cite this article as: P. S. Marrocchesi, A high energy cosmic-ray and gamma-ray observatory at the Moon South Pole: the MoonRay concept, Advances in Space Research, https://doi.org/10.1016/j.asr.2025.10.076

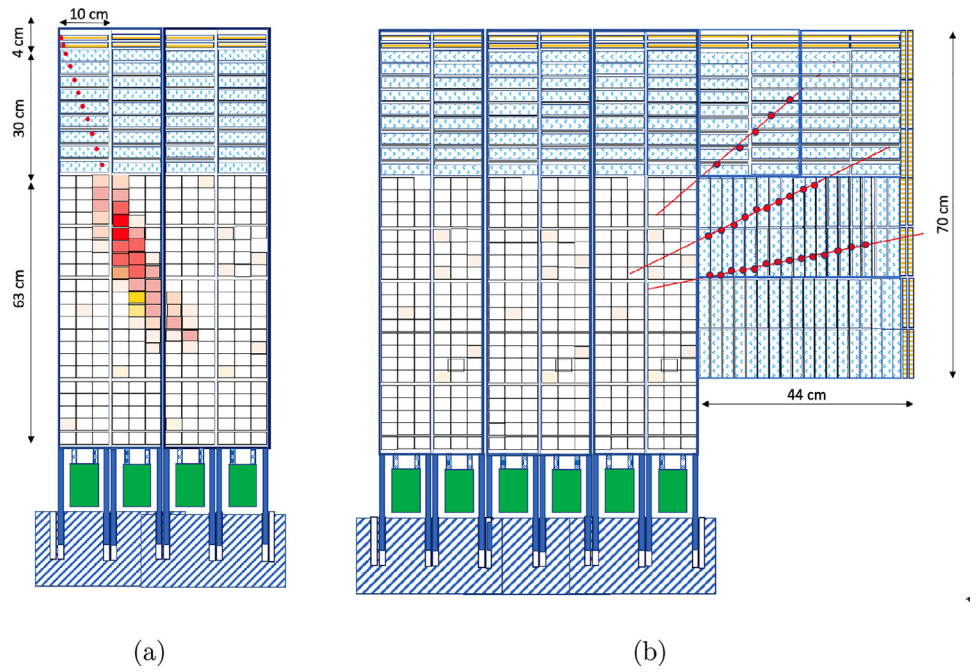

Fig. 2. (a) Artist's view of a charged track generating a shower that propagates inside two adjacent towers (each approximately 1 m high, 20 cm × 20 cm wide). (b) An example of conversion of gamma-rays at large azimuthal angle is shown (top right) in an artist's view of the concept of "horizontal towers" implemented in the "lateral walls". The latter allow for an extension of the acceptance down to a few degrees above the horizon.

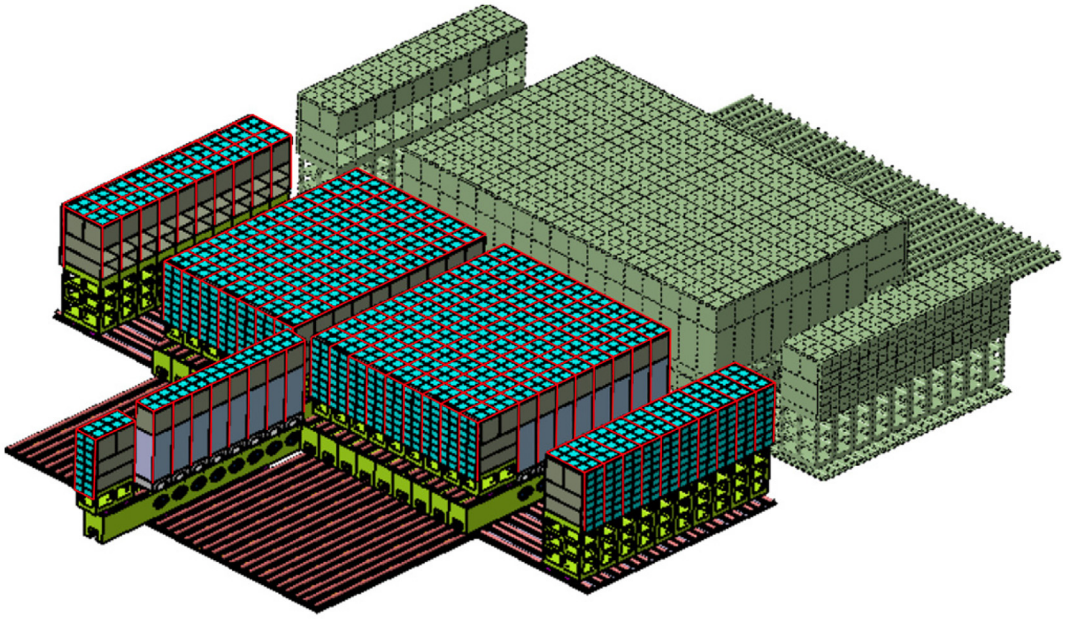

Fig. 3. Exploded view of the large telescope array configuration with 16 ×16 towers (3.2 m×3.2 m×1 m), showing the concept of tower deployment and replacement. Lateral walls are shown only along two sides.

achieved with horizontal modules that are very similar in design to the upper part of a tower. In fact they implement only the CD-ToF and Tracker sub-systems, but not the calorimeter whose functionality is already provided, at all incident angles, by the "core" of the telescope. The horizontal modules are equipped with a longer tracker, obtained by increasing the number of silicon-strip detector (SSD) layers. Hermetic coverage of the intermediate angles is provided by "short towers", equipped with extra CD-ToF layers (Fig. 2(b), top right corner). With this geometry, charge measurement and backscattering rejection is extended to all sides of the telescope and covers angles down to a few degrees above the horizon.

Please cite this article as: P. S. Marrocchesi, A high energy cosmic-ray and gamma-ray observatory at the Moon South Pole: the MoonRay concept, Advances in Space Research, https://doi.org/10.1016/j.asr.2025.10.076

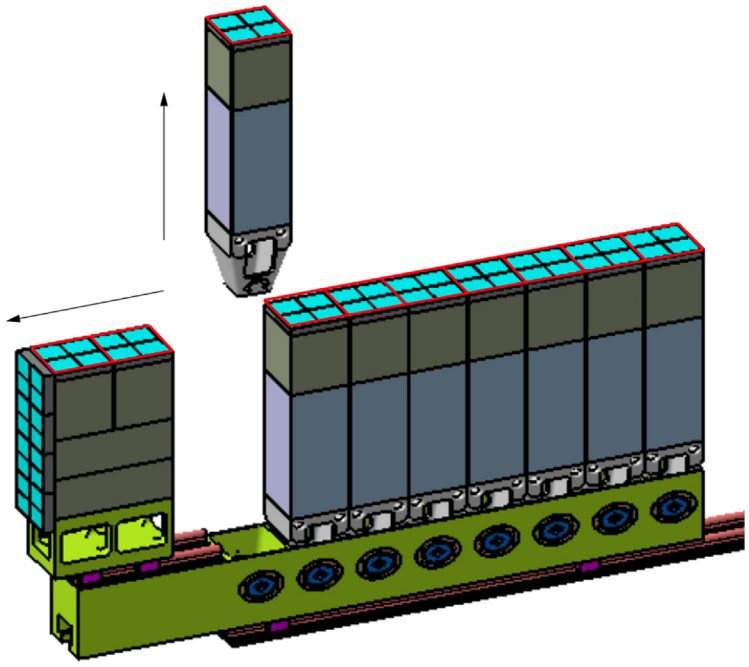

Fig. 4. Detail of a possible mechanical arrangement for the deployment/replacement of a single tower. All services (power, digital connections to trigger and readout) shall be designed in such a way that each tower can be easily replaced inside the unpressurized shed with relatived simple handling tools by astronauts wearing space suits. All repair/replacement of tower parts are carried out inside the nearby pressurized habitat.

3.1. Geometric factor and Effective Area

Two main configurations have been considered for the telescope array. In the first one (MoonRay-100), the central core of the instrument is structured into 100 towers, covering a volume of approximately $2\times2\times1$ m^3, and surrounded by lateral walls (see Fig. 3). The latter provide extra acceptance for a total geometric factor close to 11.1 m^{2}sr for protons, as detailed in Table 1. The effective acceptance for protons is estimated around 6.0 m^{2}sr, while for electrons it reaches 7.1 m^{2}sr as a complete containement for electrons of TeV energies is achieved in the first 30 radiation lengths of the bulk calorimeter, a condition easily met for inclined tracks.

Table 1
Geometric Factor (m^{2}sr) for the detection of charged cosmic rays for two configurations of the MoonRay telescope.

MOONRAY-100 10x10 towers	2x2x1 m^3	GF (m^{2}sr) (proton/electron)	GF_{eff} (m^{2}sr) **proton** 100 TeV $55X_0$	GF_{eff} (m^{2}sr) **electron** 100 TeV $30X_0$
TOP-DOWN (TD)	2x2	6.5/7.6	3.5	4.1
LATERAL (4 LT)	2x0.7	4.6/5.5	2.5	3.0
TOTAL (TD + 4 LT)		11.1/13.1	**6.0**	**7.1**

MOONRAY-256 16x16 towers	3.2x3.2x1 m^3	GF (m^{2}sr) (proton/electron)	GF_{eff} (m^{2}sr) **proton** 100 TeV $55X_0$	GF_{eff} (m^{2}sr) **electron** 100 TeV $30X_0$
TOP-DOWN (TD)	3.2x3.2	20.9/22.4	11.3	12.1
LATERAL (4 LT)	3.2x0.7	6.5/7.1	3.5	3.8
TOTAL (TD + 4 LT)		27.4/29.5	**14.8**	**15.9**

Please cite this article as: P. S. Marrocchesi, A high energy cosmic-ray and gamma-ray observatory at the Moon South Pole: the MoonRay concept, Advances in Space Research, https://doi.org/10.1016/j.asr.2025.10.076

The complete configuration (MoonRay-256) is shown in Fig. 3 with 256 towers covering a volume of approximately $3.2\times3.2\times1$ m^3. The surrounding walls allow for a total geometric factor close to 27.4(29.5) m^{2}sr for protons (electrons), as detailed in Table 1. The effective acceptance is estimated around 14.8 m^{2}sr for protons and 15.9 m^{2}sr for electrons, respectively.

3.2. The gamma-ray sky seen from the Moon South Pole

The present research gap in high-energy gamma-rays is related to a number of still unresolved, long-standing, puzzles in modern astrophysics, including the connection of gamma rays with the violent phenomena that generate CR acceleration, the nature of Dark Matter, and the origin of high energy cosmic rays.

A new generation of space-based instruments for direct gamma-ray observations at high energy started in June 2008, when the FERMI gamma-ray telescope Atwood et al. (2009) was launched. Currently in operation, it is the largest gamma-ray space-based detector ever built, to date. It employs particle physics technology and was preceded by the all-Italian pathfinder AGILE (http://agile.rm.iasf.cnr.it) launched in 2007. The satellite experiment DAMPE (Chang et al., 2017), launched in 2015, has a structure and an effective area similar to AGILE. It has a thick imaging calorimeter (~31 radiation lengths) equipped with BGO crystals, while CALET (https://calet.jp/) - launched a few months earlier of the same year and installed on the ISS - has a PWO4 based calorimeter preceded by a pre-shower, for a total of 30 radiation lengths. The proposed HERD experiment (https://herd.ihep.ac.cn/), planned for the Chinese Space Station (CSS), has been designed with a 55 radiation lengths calorimeter equipped with LYSO crystals.

The spectrum of gamma rays spans almost 7 decades in energy and about 14 in flux. The latter rapidly decreases at higher energies, therefore the instrument effective area - defined as the product of the geometrical area, times the detector efficiency - has to grow with increasing energy. However, an effective area larger than 1 m^2 is difficult to be accommodated on a spacecraft, due to mass and power constraints. The present experimental scenario calls for new observations of gamma rays, including the identification of FERMI unassociated sources, a detailed study of gamma-ray emission from the Galactic center region, identification of new sources in the Southern Hemisphere, studies of Galactic winds, investigation on the origin of the FERMI bubbles, identification of new gamma-ray pulsars, a detailed study of Vela SNR (which is known to host a pulsar), observation of binaries with strong γ-ray emission (including BH binaries) and of Active Galactic Nuclei (AGN), improved modeling of galactic γ-ray diffuse background, study of extragalactic γ-ray diffuse emission, search for narrow spectral lines as signatures of DM annihilation, study of transients (GRBs) and of the association of Gravitational Waves (GW) with their electromagnetic counterparts. The detection of gamma-rays down to shallow angles above the horizon covering the Galactic Centre, takes advantage of the lateral walls with an estimated effec-

Table 2
Effective Area (m^2) for gamma-ray detection, resulting from the convolution of acceptance and efficiency.

MOONRAY-100 10x10 towers (2m x 2m x 1m)	SSD Tiles	ε_{conv}	$\langle\varepsilon\rangle_{cuts}$	$Area_{eff}$ (m^2)
TOP-DOWN tiles (TD)	400	0.57	0.7	1.3
LATERAL tiles (LT)	4x80	0.81	0.7	1.6
CORNER tiles (CT)	4x80	0.57	0.7	1.0
TOTAL (TD + 4 LT + 4 CT)	1040			**3.9**

MOONRAY-256 16x16 towers (3.2m x 3.2m x 1m)	SSD Tiles	ε_{conv}	$\langle\varepsilon\rangle_{cuts}$	$Area_{eff}$ (m^2)
TOP-DOWN tiles (TD)	1024	0.57	0.7	3.3
LATERAL tiles (LT)	4x128	0.81	0.7	2.6
CORNER tiles (CT)	4x128	0.57	0.7	1.6
TOTAL (TD + 4 LT + 4 CT)	2048			**7.5**

Please cite this article as: P. S. Marrocchesi, A high energy cosmic-ray and gamma-ray observatory at the Moon South Pole: the MoonRay concept, Advances in Space Research, https://doi.org/10.1016/j.asr.2025.10.076

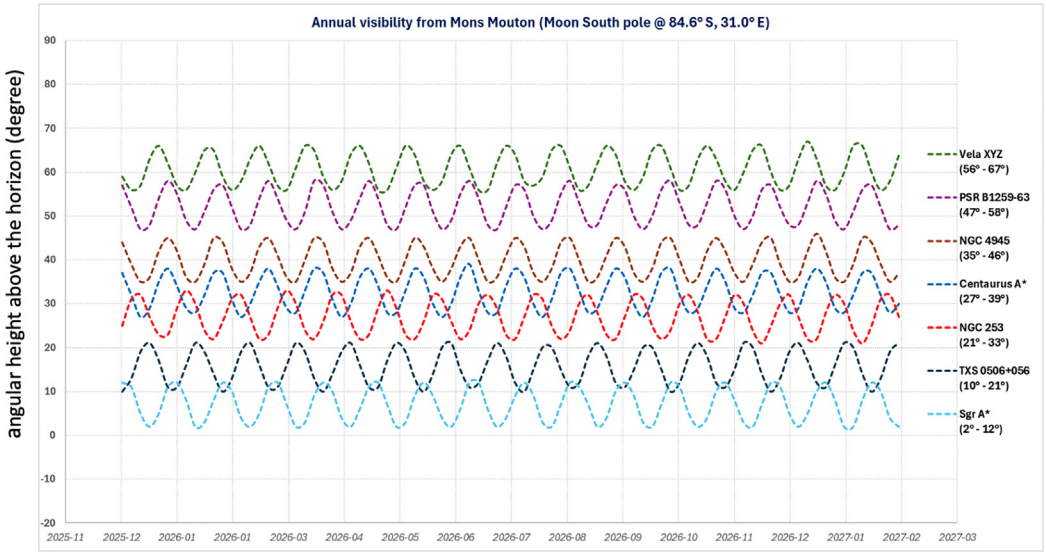

Fig. 5. Annual visibility of seven sources from a candidate site possibly located at Mount Mouton, close to the Moon South Pole, at 84.6°S latitude, 130.0°E longitude. The Galactic Center is somewhat low above the horizon, however SgrA* remains visible all along the year reaching a maximum at 12°.

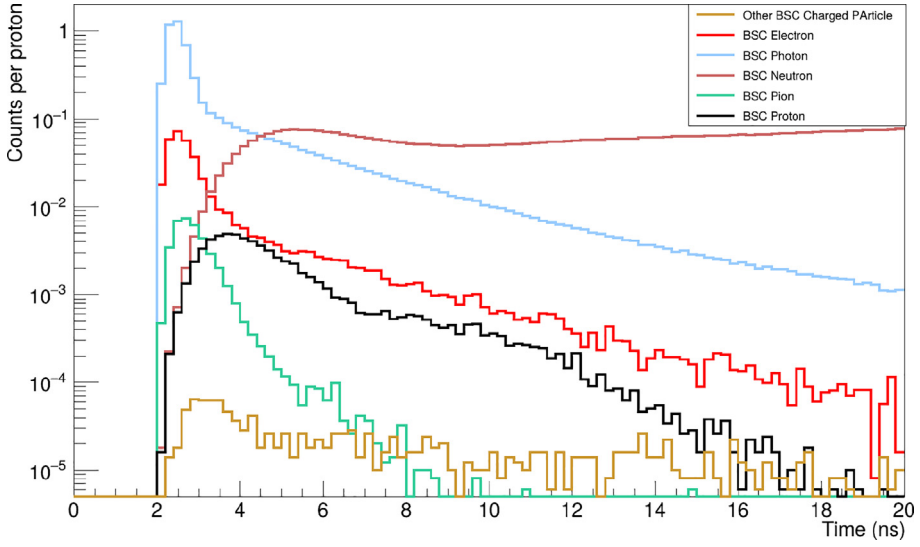

Fig. 6. GEANT4 simulation of the time-of-arrival on the CD-ToF of BSC radiation (with kinetic energy > 0.03 MeV) generated by the impact of 100 GeV protons on the calorimeter. Incoming protons first hit the charge detector at normal incidence and time $t = 0$, then reach the calorimeter at 30 cm distance. The main components of backscattered radiations include: photons (pale blue), neutrons (mauve), electrons(red), protons (black), charged pions (green) and other minor components of charged particles (brown). The horizontal scale is in ns. The vertical scale is normalized to the number of incident protons. (For interpretation of the references to colour in this figure legend, the reader is referred to the web version of this article.)

tive area (above 1 GeV) of 3.9 m^2 for MoonRay-100 and 7.5 m^2 for MoonRay-256, respectively (Table 2). As a first-order comparison with FERMI-LAT effective area of 0.9 m^2 (on axis), MoonRay-256 would represent an eightfold increase in the effective area with an on source duty cycle $\sim$ 6 times longer. With a geometric factor close to 15 m^2sr and about 8 times larger sensitive area than FERMI-LAT (Table 2), MoonRay will be able to carry out a very rich observational program over a time span of a few decades with the observation of the Southern Sky in gamma rays, from GeV to multi-TeV, from the lunar South Pole.

Assuming a candidate site, possibly located at Mount Mouton (84.6°S latitude, 130.0°E longitude), close to the Moon South Pole, the visibility above the horizon of important sources in the Southern Sky is summarized in Fig. 5 showing the expected modulation due to the lunar day, and a duty cycle of 100% for the sources considered. Unfortunately the Galactic Centre is quite low on the horizon, yet it can be traced during the whole year, provided

Please cite this article as: P. S. Marrocchesi, A high energy cosmic-ray and gamma-ray observatory at the Moon South Pole: the MoonRay concept, Advances in Space Research, https://doi.org/10.1016/j.asr.2025.10.076

the lateral walls coverage is implemented down to a few degrees.

A preliminary evaluation of the expected PSF of MoonRay as a function of energy, indicates an expected angular resolution of ~0.05° at 1 TeV, to be compared with 0.08° for FERMI and CALET, an expected 0.05° for HERD and CTAO South, and ~0.2° for LHAASO at the same energy.

4. The MoonRay instrument

4.1. The CD-ToF particle identifier

Calorimetric instruments are affected by the presence of backscattered (BSC) radiation from the calorimeter. It includes charged particles, but also photons and neutrons, back-propagating and interacting with the upstream detector material (Fig. 6) where they generate secondary ionization. The identification of the incident cosmic ray can be carried out by a precise measurement of its electric charge via a single (or multiple) dE/dx measurement(s) provided by segmented scintillators or by multi-strip/pixel silicon detectors placed at the top of the experimental apparatus. Backscattered radiation degrades the charge resolution whenever it generates background ionization falling onto the same pixel (or micro-strip, or scintillator element) hit by the incident particle. It also makes the association of hits to tracks more difficult and can downgrade the angular resolution. The problem gets worse as the energy of the primary increases as the amount of BSC albedo grows roughly as the square root of the energy.

A traditional approach to the design of charge identifiers is placing them at a reasonable stand-off distance from the calorimeter, optimizing their granularity and performing redundant charge measurements. However, a high granularity implies a large number of readout channels which is detrimental to the available power budget. A different approach exploits the difference in the time of arrival between the incident particle and the backscattered radiation hitting the detector at a later time. An example is shown in Fig. 6, taken from a GEANT4 simulation with 100 GeV protons at normal incidence on the calorimeter and a flight path L = 30 cm (the horizontal axis represents the total flight time in ns).

With this geometry, a relativistic particle takes about 1 ns to reach the calorimeter and about as much is taken by the BSC radiation to hit the charge detector (while non-relativistic BSC particles take >1 ns). Therefore an efficient rejection of the BSC background can be achieved with a "5D sensor" i.e., a pixelated instrument that can simultaneously measure the position (x,y,z), charge (q), and timing (t) of the incident particle.

A smaller flight path (down to ~10 cm) between the charge detector and the calorimeter might be chosen to increase the acceptance. In this case the ToF should achieve a sub-ns time resolution. A 10 cm distance corresponds to about 300 ps flight time for relativistic particles to reach the calorimeter and approximately the same amount of time is taken by a relativistic backscatter to reach the top of the instrument. In this case a ToF instrument with a 100 ps time resolution would allow to reject most of the BSC background to better than 5 sigma.

Avalanche detectors with an internal gain layer can achieve a better timing resolution (eventually reaching a few tens ps) than traditional silicon-strip detectors due the large slew rate dV/dt ot the signal generated by the avalanche process. The granularity of the CD-ToF instrument results from a tradoff between a minimization of the number of events with a BSC hit falling on the same pixel crossed by the incident CR particle and the power budget. The proposed implementation for MoonRay is based on pixelated LGADs with a relatively modest internal gain < 10 and with 3 mm granularity. The CD-ToF design is based on two staggered layers of LGAD pixels ensuring the availability of at least one measurement for particles crossing dead areas in one layer (or at the tower bound-

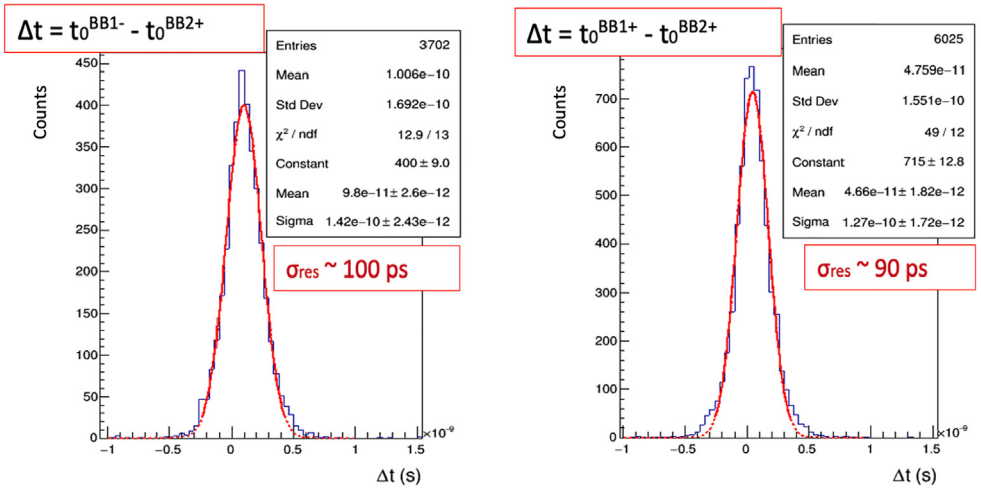

Fig. 7. Preliminary results on the time resolution measured with a prototypal LGAD array at CERN SPS ion beam test.

Please cite this article as: P. S. Marrocchesi, A high energy cosmic-ray and gamma-ray observatory at the Moon South Pole: the MoonRay concept, Advances in Space Research, https://doi.org/10.1016/j.asr.2025.10.076

aries) while providing a redundant charge measurement over most of the instrumented area.

The expected charge resolution of the Cd-ToF was simulated with GEANT4. The energy deposits in the LGAD sensor, generated by incident ultra-relativistic ions of atomic number $1 \leqslant Z \leqslant 28$, is convolved with the parameterized response of the LGAD sensor and with the simulated noise and linearity of the front-end electronics. At low Z values the charge resolution is dominated by energy straggling, while the contribution from the electronics noise becomes significant (but sub-dominant) only at $Z > 20$. Preliminary results on the expected performance of MoonRay, obtained with GEANT4 simulations, indicate that the charge identification capability provided by the CHD-ToF allows for a clean separation of individual elements from proton to $Z = 28$ (see (Marrocchesi, 2023), Fig. 3).

The timing resolution of LGAD sensors depends on several independent contributions including: jitter, time-walk, Landau noise, signal distortion, and digitization error. It has been modeled by several authors (including (Cartiglia et al., 2017; Giacomini, 2021)). The target timing resolution for MoonRay is 100 ps.

During a recent campaign at CERN (November 2024) with a beam of fragmented Pb ions, 5 layers of 3 mm×3 mm LGAD pixels (with either 150 or 275 μm thickness) were interfaced with large dynamic range front-end electronics, digitized, and read out. Each layer hosted 16 LGAD devices with 2×2 pixels each, with several configurations of guard-ring geometry and inter-pixel distance. Measurement of the timing performance were carried out with a dedicated double layer of LGAD pixels interfaced to a digital front-end circuitry connected to a high bandwidth digital oscilloscope. The preliminary results shown in Fig. 7 are consistent with a time resolution close to 100 ps.

4.2. The tracker and gamma-ray converter

In order to measure the direction of the incident particle, position sensitive detectors are arranged in layers, filling the gap between the CD-ToF and the calorimeter (MCAL). The tracker layers are interspaced with thin tungsten absorbers for the conversion of gamma rays. The threshold for gamma detection is chosen around 1 GeV. In this case the opening angle of positron–electron pairs is so small that two-track vertexing does not produce a significant improvement on the angular resolution. The latter is limited to about 0.1° for C and O nuclei above 10 GeV.

The axis of the shower is reconstructed by the imaging calorimeter with an angular resolution limited by its coarse granularity. However it is sufficient to provide a Road-of-Interest (RoI) joining the impact point of the track on the MCAL with the entrance point in the CD-ToF where spurious hits from the BSC background can be rejected thanks to the ToF. A minimum number of 4 coordinates per view from the MT are sufficient to reconstruct the incident track. The impact position resolution is modest (of the order of 150–200 μm) but sufficient. With these assumptions, a total of 8 layers of X-Y silicon strip detectors with a readout pitch of 200 μm (e.g., 100 μm pitch with a floating strip) could be implemented with 4 wafers (~10 cm×10 cm, each) per layer.

The relative alignment of the towers is not a critical issue for the tracking, but in principle it could degrade the angular resolution for gamma-ray measurements (please note that MoonRay detects gamma-rays above 1 GeV and it is not required to reconstruct electron–positron pairs, like Fermi does, at lower energies). In any case, the mechanical arrangement that has been envisaged so far, leaves enough tolerance for the towers to be inserted in the array, but - once inserted - their positions are locked into calibrated positions resulting in a rigid assembly not so dissimilar from FERMI LAT. Residual systematic (or temperature related) misalignments will be corrected via continuous and extensive tracking calibrations.

4.3. The 3D-imaging calorimeter

The incident energy is measured by a homogeneous calorimeter (MCAL) with imaging capabilities. In order to achieve a 3D view of the showers and to fully exploit the additional solid angle coverage provided by the lateral walls, the calorimeter is segmented into a 3D array of scintillating crystal cubes with 3 cm side. The chosen granularity matches the Molière radius R_M of the crystal, a parameter governing the transverse lateral development of electromagnetic (e.m.) showers.

In order to fully contain the longitudinal development of e.m. showers at TeV energies and to minimize the energy leaks of hadronic showers in the multi-TeV domain, a deep calorimeter is needed. The present design figure corresponds to an equivalent depth of 55 X_0 (radiation lengths).

Assuming LYSO(Ce) ($X_0 = 1.14$ cm, $R_M = 2.1$ cm) as the scintillating crystal, each tower would consist of 756 crystals arranged in 21 vertical layers with 36 crystals per layer, for a total height of 63 cm (not including spacers) and a weight of ~150 (25) kg under Earth (Moon) gravity (see Fig. 2). For a track at normal incidence, the total thickness of a tower corresponds to about 3 proton interaction lengths λ_I. Above 100 GeV the energy dependence of the resolution is expected to level to a constant term of the order of 1–2% for electrons, which ultimately depends on the accuracy in the construction, calibration, and stability of the calorimeter. A proton/electron discrimination of 10^5 is expected. This is achieved mainly by leveraging on the 3D imaging capabilities of the calorimeter and the application of topological cuts based on the different shapes of e.m. versus hadronic showers. The expected average energy resolution for a baseline design with 100 towers is around 30% for protons, approximately scaling as $A^{-1/2}$ for nuclei with mass number A.

The huge dynamic range of the calorimetric energy deposits, spans from a threshold of 0.3 m.i.p. to ~ 5 10^6 m.i.p. In order to cover the full range, each crystal is read-

Please cite this article as: P. S. Marrocchesi, A high energy cosmic-ray and gamma-ray observatory at the Moon South Pole: the MoonRay concept, Advances in Space Research, https://doi.org/10.1016/j.asr.2025.10.076

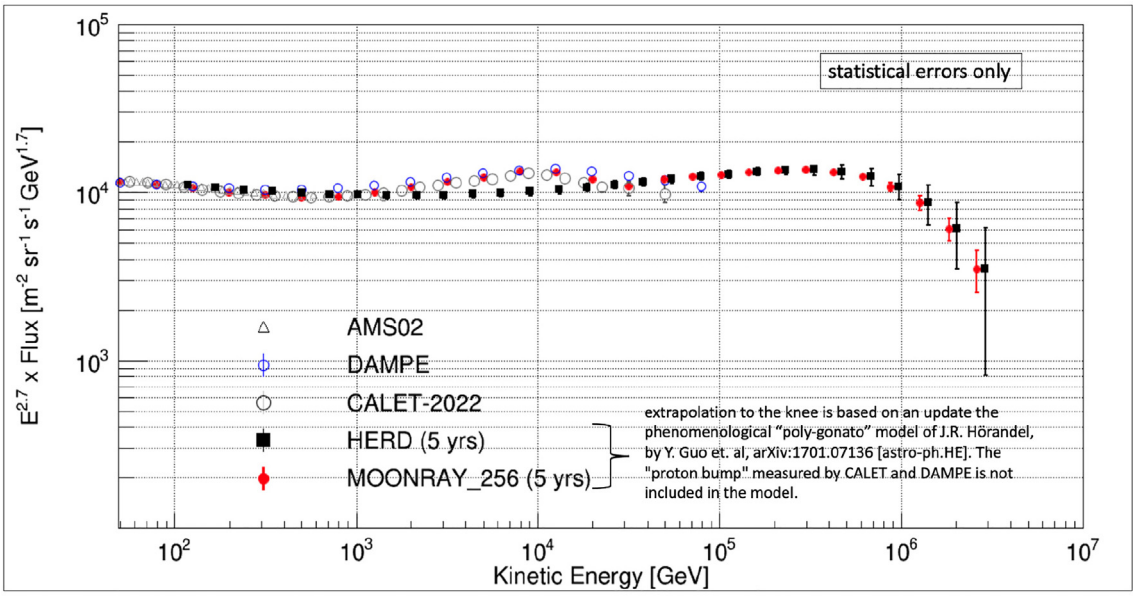

Fig. 8. Expected proton spectrum measurement with 5 years of observations with MoonRay-256 together with a (partial) compilation of existing measurements up to the 100 TeV scale. The extrapolation to the knee region is model dependent. Only statistical errors are shown.

out by two photosensors (e.g., photodiodes) with different sensitive areas, coupled to multi-range front-end electronics. The readout electronics interface is located at the base of each tower. Special care has to be taken in the design to minimize the amount of inter-crystal gaps and of the passive material at the lateral walls of each tower, while ensuring mechanical stiffness for the insertion or replacement of each unit (Fig. 4).

5. Expected performance and design studies

As a case study, a GEANT4 simulation of the expected measurement of the proton flux after 5 years of observations with MoonRay is shown in Fig. 8 (red filled circles) where it is compared with a (partial) compilation of available experimental points in the energy range from 50 GeV to 100 TeV. The differential proton flux in kinetic energy E is multiplied by $E^{2.7}$. The simulation is based on a MoonRay configuration with 16×16 towers. Error bars are representative of statistical errors only. A dramatic improvement with respect to the currently available data from direct measurements can be seen on the picture. This excellent performance is largely driven by an increase (by almost two orders of magnitude) of the exposure with MoonRay, which would allow for a more precise determination of the spectral anomalies of proton and helium fluxes (as well as of heavier ions) and an extension of the measurements into the uncharted region beyond a few hundred TeV.

At even higher energies, we can only make an educated guess on the shape of the proton flux at the PeV scale. In this region, available data are based on ground observations and affected by large systematic errors on the flux and on the elemental composition. With the above caveats, we estimated the flux sensitivity for proton and He above 100 TeV, as shown in Fig. 8, assuming a MoonRay configuration with 256 towers and 5 years of observations. The extrapolation to knee energies is based on the phenomenological model of (Hörandel, 2003). Please note that the above model was implemented well before the discovery of the "proton bump", therefore in Fig. 8 we also show the data points measured by CALET in the bump region. This study suggests that MoonRay can bridge the gap from the 100 TeV scale to the knee (Fig. 8) and establish the elemental composition at the PeV scale.

Possible alternatives to the present design of MCAL are being studied in order to increase the aspect ratio of the calorimeter, a limiting factor for the geometrical factor (GF) of the whole instrument.

6. Power budget, thermal control, data downlink, cost

In this section we mention a few critical technical aspects of the project. A detailed risk assessment is outside the scope of the present paper.

The power required for the analog and digital electronics of the 256 array has been estimated (on the basis of realistic specifications of the main components) to be around 10–11 kW. However extra power is needed: (1) for the heaters when the temperature drops during period of scarce illumination; (2) for data transmission to Earth. The first issue largely depends on the choice of the site. Some areas within ~1–2 km of Mont Mouton candidate site are among the most sunlit spots in proximity of the lunar South Pole. The soil temperature is estimated to vary between 250–285 K during the extended sunlit periods, while during weeks of shadow or grazing illumination can reach a minimum of 80–100 K, well above the temperatures expected

Please cite this article as: P. S. Marrocchesi, A high energy cosmic-ray and gamma-ray observatory at the Moon South Pole: the MoonRay concept, Advances in Space Research, https://doi.org/10.1016/j.asr.2025.10.076

at Permanently Shadowed Regions (PSRs), at the bottom of craters, attaining 40 K. A quantitative estimate of the power required for thermal control, and the assessment of survival operative limits, during prolonged periods of power loss, needs a full thermal model and depends on the final choice of the lunar site.

Constant data flow between the experiment and Earth, for control and data downlink, will have to be maintained. The required bandwidth can be estimated in the ball park, based on the expected trigger rate and event size, with a required downlink capability below 10 GB/day (to be compared with 12.75 GB/day estimated for HERD). The impact of these requirements on the communication network in terms of power budget has to be determined.

While it is quite clear that the cost per kg to send anything to the Moon is, at present, so large to be dominant with respect to construction costs, it may be useful to remark that the cost of the crystals of the homogeneous calorimeter is the largest contribution to the total budget estimate of each tower. Therefore a different choice of crystals, other than LYSO, in under study in consideration of their high costs (at market price). One possible alternative is the less luminous BGO, which might require more sensitive photodetectors to achieve the required signal-to-noise ratio for the detection of the lighest nuclei.

7. Conclusions

A conceptual approach towards the design of a lunar CR telescope was summarized in this paper. The implementation of a multi-ton instrument on the Moon is out of question unless a modular approach is followed. A possible scheme, based on relatively small and lightweight independent modules, is being addressed by the MoonRay project with the development of innovative sensors and high energy instrumentation that were briefly introduced in the sections dedicated to the CD-ToF and MCAL.

The scope of this paper is limited to a preliminary concept study of MoonRay. We do not address here important questions related to systematic effects, nor discuss in detail the sensitivity of the instrument to high energy gamma rays. An innovative CD-ToF system was described that can reject most of the BSC background from the calorimeter thus improving charge identification. Backscatters can also cause fake veto signals in the anti-coincidence system for gamma-ray detection. The design of the latter is not included in the present study.

At the time of writing, the design of the towers is still at a preliminary stage, while an active detector development of the LGAD arrays and of the associated front-end electronics is being pursued in Italy in the framework of the R&D activities of the Istituto Nazionale di Fisica Nucleare (INFN). Preliminary beam test results of a prototype array were reported in the paper.

Given the large breath of the project, a final remark is in order. While it is difficult to predict whether cosmic radiation observatories on the Moon may receive attention and substantial funding in the near future, the assumption of a possible presence of human habitats on the Moon is not unrealistic on a longer time scale. Therefore we believe that a thorough concept study of MoonRay should be pursued.

Declaration of Competing Interest

The authors declare that they have no known competing financial interests or personal relationships that could have appeared to influence the work reported in this paper.

Acknowledgements

The author would like to acknowledge the support of Istituto Nazionale di Fisica Nucleare for the ongoing development of the CD-ToF sensors, and of the University of Siena and INFN-Pisa for the computer resources used for the simulations. We would like to thank CERN for the beam line allocation and smooth operations during the test. We also acknowledge the contribution of Marco Mattiazzi for the geometric factor calculations, of Mina Maghami Moghim for the BSC time-of-flight simulation, and of Alessandro Marchini for the tracking of astrophysical sources at Mont Mouton.

References

Adriani, O., Barbarino, G.C., Bazilevskaya, G.A., et al., 2011. PAMELA measurements of cosmic-ray proton and helium spectra. Science 332, 69–72. https://doi.org/10.1126/science.1199172.

Adriani, O., Akaike, Y., Asano, K., et al., 2019. Direct measurement of the cosmic-ray proton spectrum from 50 GeV to 10 TeV with the calorimetric electron telescope on the International Space Station. Phys. Rev. Lett. 122, 181102. https://doi.org/10.1103/PhysRevLett.122.181102.

Adriani, O., Akaike, Y., Asano, K., et al., 2022. Observation of spectral structures in the flux of cosmic-ray protons from 50 GeV to 60 TeV with the calorimetric electron telescope on the International Space Station. Phys. Rev. Lett. 129, 101102. https://doi.org/10.1103/PhysRevLett.129.101102.

Adriani, O., Altomare, C., Ambrosi, G., et al., 2022. Design of an antimatter large acceptance detector in orbit (ALADInO). Instruments 6 (2), 19. https://doi.org/10.3390/instruments6020019.

Aguilar, M., Aisa, D., Alpat, B., et al., 2015. Precision measurement of the proton flux in primary cosmic rays from rigidity 1 GV to 1.8 TV with the alpha magnetic spectrometer on the International Space Station. Phys. Rev. Lett. 114, 171103. https://doi.org/10.1103/PhysRevLett.114.171103.

Aguilar, M., Ali Cavasonza, L., Ambrosi, G., et al., 2020. Properties of neon, magnesium, and silicon primary cosmic rays results from the alpha magnetic spectrometer. Phys. Rev. Lett. 124, 211102. https://doi.org/10.1103/PhysRevLett.124.211102.

Ahn, H.S., Allison, P., Bagliesi, M.G., et al., 2010. Discrepant hardening observed in cosmic-ray elemental spectra. Astrophys. J. Lett. 714, L89–L93. https://doi.org/10.1088/2041-8205/714/1/L89.

Aloisio, R., Blasi, P., 2013. Propagation of galactic cosmic rays in the presence of self-generated turbulence. J. Cosmol. Astropart. Phys. 07, 001. https://doi.org/10.1088/1475-7516/2013/07/001.

An, Q., Asfandiyarov, R., Azzarello, P., et al., 2019. Measurement of the cosmic ray proton spectrum from 40 GeV to 100 TeV with the DAMPE satellite. Science Adv. 5 (9). https://doi.org/10.1126/sciadv.aax3793.

Please cite this article as: P. S. Marrocchesi, A high energy cosmic-ray and gamma-ray observatory at the Moon South Pole: the MoonRay concept, Advances in Space Research, https://doi.org/10.1016/j.asr.2025.10.076

Atkin, E., Bulatov, V., Dorokhov, V., et al., 2018. New universal cosmic-ray knee near a magnetic rigidity of 10 TV with the NUCLEON space observatory. JETP Lett. 108, 5–12. https://doi.org/10.1134/S0021364018130015.

Atwood, W.B., Abdo, A.A., Ackermann, M., et al., 2009. The large area telescope on the Fermi gamma-ray space telescope mission. Astrophys. J. 697, 1071–1102. https://doi.org/10.1088/0004-637X/697/2/1071.

Bernard, G., Delahaye, T., Keum, Y.-Y., 2013. TeV cosmic-ray proton and helium spectra in the myriad model. Astron. Astrophys. 555, A48, DOI:10.1051/0004-6361/201321202.

Blasi, P., Amato, E., Serpico, P.D., 2012. Spectral breaks as a signature of cosmic ray induced turbulence in the galaxy. Phys. Rev. Lett. 109, 061101. https://doi.org/10.1103/PhysRevLett.109.061101.

Caprioli, D., Haggerty, C., Blasi, P., 2021. The theory of efficient particle acceleration at shocks. PoS 482, 482. https://doi.org/10.22323/1.395.0482 (ICRC2021).

Cartiglia, N., Arcidiacono, R., Baldassarri, B., et al., 2017. Tracking in 4 dimensions. Nucl. Instr. Methods A 845, 47–51. https://doi.org/10.1016/j.nima.2016.05.078.

Chang, J., Ambrosi, G., An, Q., et al., 2017. The dark matter particle explorer mission. Astropart. Phys. 95, 6–24. https://doi.org/10.1016/j.astropartphys.2017.08.005.

Cristofari, P., Blasi, P., Caprioli, D., 2022. Microphysics of diffusive shock acceleration: impact on the spectrum of accelerated particles. Astrophys. J., 930:28, DOI 10.3847/1538-4357/ac6182.

Dong, Y., Xu, M., Wang, Z., et al., 2018. A novel 3-D calorimeter for the High Energy cosmic-Radiation Detection (HERD) Facility onboard China's Future Space Station. PoS ICRC2017 253, DOI: 10.22323/1.301.0253.

Evoli, C., Amato, E., Blasi, P., et al., 2021. Stochastic nature of Galactic cosmic-ray sources. Phys. Rev. D 104, 123029. https://doi.org/10.1103/PhysRevD.104.123029.

Giacomini, G., 2021. Fabrication of silicon sensors based on low-gain avalanche diodes. Front. Phys. 9, 618621. https://doi.org/10.3389/fphy.2021.618621.

Hörandel, J.R., 2003. On the knee in the energy spectrum of cosmic rays. Astropart. Phys. 19, 193–220. https://doi.org/10.1016/S0927-6505(02)00198-6.

Kawanaka, N., Yanagita S., S., 2018. Cosmic-ray lithium production at the nova eruptions followed by a type IA supernova. Phys. Rev. Lett. 120, 041103. https://doi.org/10.1103/PhysRevLett.120.041103.

Lipari, P., Vernetto, S., 2025. Resolved and unresolved Galactic gamma-ray sources. Phys. Rev. D 111, 063035. https://doi.org/10.1103/PhysRevD.111.063035.

Malkov, M., Moskalenko, I., Diamond, P., et al., 2024. Very local impact on the spectrum of cosmic-ray nuclei below 100 TeV. Adv. Space Res. 74 (9), 4264–4275. https://doi.org/10.1016/j.asr.2024.08.060.

Marrocchesi P.S., P.S., 2023. MOONRAY: A permanent high-energy cosmic-ray observatory on the surface of the Moon. Astropart. Phys. 152, 102879. https://doi.org/10.1016/j.astropartphys.2023.102879.

Panov, A.D., Adams, J.H., Ahn, H.S., et al., 2007. The results of ATIC-2 experiment for elemental spectra of cosmic rays. Bull. Russ. Acad. Sci. Phys. 71, 494–497. https://doi.org/10.3103/S1062873807040168.

Schael, S., Atanasyan, A., Berdugo, J., et al., 2019. AMS-100: The next generation magnetic spectrometer in space – An international science platform for physics and astrophysics at Lagrange point 2. Nucl. Instr. Methods A 944, 162561. https://doi.org/10.1016/j.nima.2019.162561.

Thoudam, S., Hörandel, J., 2014. GeV-TeV cosmic-ray spectral anomaly as due to reacceleration by weak shocks in the Galaxy Astron. Astrophys. 567, A33. https://doi.org/10.1051/0004-6361/201322996.

Tomassetti, N., 2015. Origin of the spectral upturn in the cosmic-ray C/Fe and O/Fe ratios. Phys. Rev. D 92, 063001. https://doi.org/10.1103/PhysRevD.92.063001.

Vladimirov, A.E., Jóhannesson, G., Moskalenko, I.V., et al., 2012. Testing the origin of high-energy cosmic rays. Astrophys. J. 752, 68. https://doi.org/10.1088/0004-637X/752/1/68.

Zatsepin, V.I., Sokolskaya, N.V., 2006. Three component model of cosmic ray spectra from 10 GeV to 100 PeV. Astron. Astrophys. 458, 1–5. https://doi.org/10.1051/0004-6361:20065108.

Please cite this article as: P. S. Marrocchesi, A high energy cosmic-ray and gamma-ray observatory at the Moon South Pole: the MoonRay concept, Advances in Space Research, https://doi.org/10.1016/j.asr.2025.10.076